


<b>Titre:</b> Title:	Investigating the impact of drill material on hole quality in jute/palm fiber reinforced hybrid composite drilling with uncertainty analysis
<b>Auteurs:</b> Authors:	Mohamed Slamani, Abdelmalek Elhadi, Salah Amroune, Mustapha Arslane, Walid Jomaa, Hassan Fouad, Jean-François Châtelain, & Mohammad Jawaid
<b>Date:</b>	2024
<b>Type:</b>	Article de revue / Article
<b>Référence:</b> Citation:	Slamani, M., Elhadi, A., Amroune, S., Arslane, M., Jomaa, W., Fouad, H., Châtelain, J.-F., & Jawaid, M. (2024). Investigating the impact of drill material on hole quality in jute/palm fiber reinforced hybrid composite drilling with uncertainty analysis. Heliyon, 10(17), e36925 (23 pages). <a href="https://doi.org/10.1016/j.heliyon.2024.e36925">https://doi.org/10.1016/j.heliyon.2024.e36925</a>

 **Document en libre accès dans PolyPublie**  
Open Access document in PolyPublie

<b>URL de PolyPublie:</b> PolyPublie URL:	<a href="https://publications.polymtl.ca/59427/">https://publications.polymtl.ca/59427/</a>
<b>Version:</b>	Version officielle de l'éditeur / Published version Révisé par les pairs / Refereed
<b>Conditions d'utilisation:</b> Terms of Use:	CC BY

 **Document publié chez l'éditeur officiel**  
Document issued by the official publisher

<b>Titre de la revue:</b> Journal Title:	Heliyon (vol. 10, no. 17)
<b>Maison d'édition:</b> Publisher:	Elsevier
<b>URL officiel:</b> Official URL:	<a href="https://doi.org/10.1016/j.heliyon.2024.e36925">https://doi.org/10.1016/j.heliyon.2024.e36925</a>
<b>Mention légale:</b> Legal notice:	© 2024 The Authors. Published by Elsevier Ltd. This is an open access article under the CC BY license ( <a href="http://creativecommons.org/licenses/by/4.0/">http://creativecommons.org/licenses/by/4.0/</a> )

# A finite-state machine-based control design for thermal and state-of-charge balancing of lithium iron phosphate battery using flyback converters

Asal Zabetian-Hosseini<sup>1</sup>  | Amin Ghazanfari<sup>2,3</sup> | Benoit Boulet<sup>1</sup>

<sup>1</sup>Electrical and Computer Engineering Department, McGill University, Montreal, Québec, Canada

<sup>2</sup>Hydro-Quebec Center of Excellence in Transportation Electrification and Energy Storage, Varennes, Québec, Canada

<sup>3</sup>Department of Electrical Engineering, Polytechnique Montréal, Montreal, Québec, Canada

## Correspondence

Asal Zabetian-Hosseini, Electrical and Computer Engineering Department, McGill University, Montreal, QC, Canada.

Email: asal.zabetian-hosseini@mail.mcgill.ca

## Funding information

Hydro-Quebec Center of Excellence in Transportation Electrification and Energy Storage, Grant/Award Number: MITAC Award IT26874

## Abstract

Battery cell balancing plays a vital role in maximizing the performance of the battery system by enhancing battery system capacity and prolonging the battery system life expectancy. Active cell balancing using power converters is a promising approach to maintaining uniform state of charges (SoCs) and temperatures across battery cells. The SoC balancing function in the battery management system (BMS) increases the battery pack capacity, and the temperature balancing function mitigates variations in the aging of battery cells due to unbalanced temperatures. In this work, a finite-state machine-based control design is proposed for lithium iron phosphate (LFP) battery cells in series to balance SoCs and temperatures using flyback converters. The primary objective of this design is to ensure balanced SoCs by the end of the charging session while mitigating the temperature imbalance during the charging process. To achieve the SoC and temperature balancing functions using the same balancing circuits, a finite-state machine control design decides on the operating mode, and a balancing strategy balances either temperature or SoC depending on the operating mode. The proposed control design has the advantages of low computational burden, simple implementation compared to the optimization-based controller found in the literature, and the proposed balancing strategy offers faster balancing speed compared to conventional methods. The effectiveness of the proposed strategy is validated on battery cell RC models in series with unbalanced SoCs and temperatures.

## KEYWORDS

battery model, finite-state machine, flyback, state-of-charge balancing, temperature balancing

This is an open access article under the terms of the Creative Commons Attribution License, which permits use, distribution and reproduction in any medium, provided the original work is properly cited.

© 2024 The Authors. *Battery Energy* published by Xijing University and John Wiley & Sons Australia, Ltd.

## 1 | INTRODUCTION

Lithium-ion batteries (LIBs) are widely utilized across various applications due to their high energy density and extended lifespan, ranging from small-scale portable devices to large-scale battery packs powering electric vehicles (EVs) and energy storage systems. The key components of LIB cells include the cathode (positive electrode, e.g., lithium cobalt oxide [LiCoO<sub>2</sub>], lithium manganese oxide [LiMn<sub>2</sub>O<sub>4</sub>], or lithium iron phosphate [LiFePO<sub>4</sub>]), anode (negative electrode, typically graphite), separator (a thin layer that isolates the cathode from the anode), electrolyte (a conductive solution with lithium salt facilitating ion transport), and current collectors (conductive materials like aluminum and copper for current transfer). The cathode material plays a pivotal role in determining the performance of LIB cells, impacting crucial aspects such as voltage, energy density, charge/discharge rates, safety, cost, and longevity. LIB battery cells with LiFePO<sub>4</sub> as a cathode (lithium iron phosphate [LFP] battery cells) has gained more attention due to their improved safety and lower cost compared to the other oxide cathodes. They are also known for their high rate performance which is a critical characteristic for fast charging of batteries.<sup>1</sup> Considering the above characteristics, LFP battery cells are commonly used in the battery packs of EVs. The EV battery pack includes hundreds of battery cells in series and parallel and accounts for a significant part of the EV production price. Research in Altaf et al.<sup>2</sup> shows the imbalance in the temperatures, and state of charges (SoCs) of the LIB battery cells can compromise safety and significantly affect the lifespan of an EV battery pack. The imbalance in SoCs mitigates the available battery pack capacity and the imbalance in temperatures of cells results in nonuniform cell aging. These issues contribute to the battery pack's capacity fading.<sup>3</sup> Although battery packs are equipped by the battery thermal management system that can maintain a suitable temperature during short-term charging operation to a certain extent, they cannot compensate for the temperature imbalance among battery cells due to the poor temperature measurement accuracy and uniform distribution of thermal management system.<sup>4</sup>

Battery pack in an EV accounts for a significant part of the EV production price. The imbalances in the temperatures and SoCs of battery cells can compromise safety and significantly affect the lifespan of an EV battery pack.<sup>2</sup> The imbalance in SoCs mitigates the available battery pack capacity, whereas the imbalance in temperatures of cells results in nonuniform cell aging. These issues contribute to the battery pack's capacity fading.<sup>3</sup> Two causes of the SoC and temperature

imbalances in battery cells are parameter variations among cells and cell locations in the battery pack. Despite significant efforts to ensure parameters of cells manufactured in the same batch are similar, studies show cell parameters (e.g., internal resistance and open-circuit voltage) can vary by more than 1%.<sup>5</sup> Variations in cell parameters exacerbate differences among cells and cause inhomogeneous voltage, SoC, and temperature over time.<sup>6–8</sup> The battery cell heat transfer capability is affected by its location in the battery pack which exacerbates the temperature imbalance among cells.<sup>9</sup> Studies such as those in Leng et al.,<sup>10</sup> and Kremer et al.<sup>11</sup> focus on the impacts of temperature on battery cell aging over numerous cycles. The findings in Leng et al.,<sup>10</sup> and Kremer et al.<sup>11</sup> reveal that temperature disparities contribute to uneven aging among cells, thereby perpetuating temperature imbalances.<sup>9</sup>

The battery pack is under the control of a battery management system (BMS) which monitors and supports the cell balancing functionality. To address the SoC imbalance issue, there are two balancing approaches implemented in the BMS: (1) passive balancing and (2) active balancing according to Naguib et al.<sup>7</sup> The passive balancing approach includes fixed resistors or switched resistors. It has the advantages of easy implementation and low cost. However, it suffers from low balancing speed and can prove inefficient by causing energy loss which contributes to the increase in the temperature of the battery pack. Passive balancing is proven to be a better balancing approach in applications with several hundred to thousand smaller capacity battery cells. Yet, when the number of series cells is smaller and the cell capacity is larger, the active balancing approach is a better alternative to passive balancing despite its more complexity and cost due to its faster balancing speed, better efficiency, and more control ability.<sup>8,9</sup> Additionally, active balancing can improve the battery pack's longevity when used for balancing the temperatures of cells. Outcomes presented in Kremer et al.<sup>11</sup> showcase that a temperature imbalance of 12.4 K can substantially influence battery longevity, and through active balancing strategies, the battery life cycle can be extended by up to 19.8%.

Naguib et al.,<sup>7</sup> Yildirim et al.,<sup>8</sup> and Omariba et al.<sup>12</sup> classify active balancing into four categories based on the component used in the balancing circuits: (1) capacitor-based balancing,<sup>13</sup> (2) inductor-based balancing,<sup>13</sup> (3) transformer-based balancing,<sup>14</sup> and (4) power converter-based balancing. The capacitor-based method in Evzelman et al.<sup>13</sup> and inductor-based balancing method in Evzelman et al.<sup>13</sup> are relatively efficient and cost-effective. Yet, the capacitor-based method suffers from a long balancing time, and the inductor-based method in

Evezlman et al.<sup>13</sup> is impacted by the high switch current stress. The transformer-based balancing in Imtiaz et al.<sup>15</sup> can be categorized in the power converter-based balancing method as well since they use topologies similar to flyback converters. These methods can provide more flexibility in balancing several states among cells due to their fast balancing capability and more control ability. In power converter-based methods, the most common power converters used for balancing are buck-boost, Ćuk, full-bridge, flyback, and quasi-resonant converters. Due to the variety in the balancing methods including power converter-based balancing methods, Ghaeminezhad et al.<sup>9</sup> studies the balancing strategies at the systematic level. Based on this study, power converter-based balancing are categorized into adjacent-based, nonadjacent-based, and direct cell-cell methods. Adjacent-based and direct cell-cell methods have a long balancing time if the unbalanced cells are not close to each other.<sup>15</sup> Nonadjacent methods can be cell-to-pack (C2P), pack-to-cell (P2C), and cell-to-pack-to-cell and provide relatively faster balancing time. However, P2C cannot provide temperature balancing without increasing the temperature of the cells, and cell-to-pack-to-cell requires more complex power converter designs. Therefore, C2P in nonadjacent methods is considered in this study.

Among different power electronic converters used for balancing strategies, the full-bridge converter connects to each cell directly which is not efficient for a battery pack with a large number of cells; the Ćuk converter has a relatively complex control design; the buck-boost converter has a limited voltage conversion level which is not proper for nonadjacent methods. The flyback converter, on the other hand, is an alternative version of the buck-boost converter with a high-frequency transformer for higher voltage conversion levels. It has the advantages of relatively high efficiency, less control complexity, fast balancing speed, and high voltage conversion level for the nonadjacent strategies.<sup>9</sup> Different topology designs of flyback converters are investigated for cell balancing in several studies.<sup>15–19</sup> Applications of a single flyback converter with multiwinding on the primary side and single winding on the secondary side are studied in Imtiaz et al.,<sup>15</sup> and Einhorn et al.<sup>16</sup> These studies show the advantages of using flyback converters for cell balancing including requiring fewer components. However, single flyback converter designs with multiwinding on the primary side in have a longer balancing time since they can balance only one cell at a time. Therefore, among different flyback converter designs, unidirectional flyback converters with a single winding for both primary and secondary sides are selected in C2P mode due to faster balancing time and capability of temperature balancing during the battery pack charging process.

The concept of temperature balancing is discussed in Refs. 2, 11, 18, 20–22 Wu et al.<sup>18</sup> and Li and Han<sup>22</sup> discuss the temperature balancing among cells in series without considering the SoC balancing. Altaf and Egardt,<sup>20</sup> Altaf et al.<sup>21</sup> introduce the concept of temperature and SoC balancing, simultaneously using full-bridge converters connected to each cell. In the method in Altaf et al.,<sup>21</sup> each cell is isolated from the rest of the battery module by the power converter which controls the voltage and current of the cell. The method is costly and very inefficient due to requiring switches with high power tolerance and requiring the operation of power converters at all times. This study attempts to address the balancing issue among temperature and SoC of battery cells by proposing a new balancing control design using the bidirectional flyback converter topology in C2P mode. Our contribution to this work can be summarized as follows:

- a finite-state machine design for cell balancing is proposed to enable the simultaneous balancing of SoC and temperature;
- balancing algorithms are proposed for SoC and temperature with simple implementation and robust performance avoiding the complex optimization-based solutions in the literature;
- a battery cell electrothermal model including a first-order electric circuit model (ECM) is developed to estimate SoC and temperature, respectively;
- a unidirectional flyback power converter in discontinuous current mode (DCM) is designed as a cell balancing circuit for each cell in the C2P mode, and its average model is developed to reduce the simulation time of cell balancing scenarios.

This paper is organized as follows: Sections 2 and 3 discuss the battery cell model and the cell balancing flyback converter design, respectively. Section 4 provides the balancing circuit control design including the proposed finite-state machine-based balancing control design to address unbalanced temperatures and SoCs and the proposed balancing strategy. Finally, Section 5 presents the case studies and results.

## 2 | BATTERY CELL MODEL DESIGN

To initiate cell balancing, the preliminary step involves battery cell modeling, which is the focus of this section. The battery cell model is designed to anticipate and replicate the battery cell's behavior during both charge and discharge processes. Its primary function is to

estimate the SoC and temperature of battery cells. Various types of battery modeling are documented in the literature.<sup>23–26</sup> These models can be broadly categorized into four types based on the physical insight: (1) electrochemical models, (2) mathematical models, (3) data-driven models, and (4) circuit-oriented models. Electrochemical models provide an intricate depiction of battery chemistry through nonlinear differential equations. Despite their high accuracy, these models have substantial computational cost. They are useful when complete observability of battery states and an understanding of microscopic scale behavior are essential. Mathematical models, on the other hand, represent the battery behavior at the system level through math-based stochastic models. Although these models offer lower accuracy, they are suitable for system-level studies. Data-driven models adopt a black box approach, utilizing machine learning algorithms to predict actual battery cell behaviors. While they provide highly accurate SoC predictions, these models need a significant amount of data and may provide out-of-range responses due to the inherent nature of black box modeling. Circuit-oriented modeling provides a balance between accuracy and computational efficiency for online applications, accurately representing battery cell features with limited data sets. An example of circuit-oriented modeling is the electrothermal model, which integrates thermal and electrical aspects to consider the mutual influence of SoC and temperature, enhancing battery model accuracy.<sup>23,26</sup> Consequently, the electrothermal battery cell model is chosen for estimating SoC and temperature variations due to its favorable combination of low computational complexity and high accuracy. The

electrothermal battery cell model combines a battery cell's ECM and thermal model as shown in Figure 1.

## 2.1 | Electrical circuit model design

A Thevenin-based ECM is used for this study for the battery cell model. In this model, the transient responses of battery cells are captured by a series interconnection of parallel resistor-capacitor (RC) pairs. RCs mimic the transient and steady-state behaviors of the battery cell. Comparing the accuracy of different numbers of RCs in the model, an ECM with one pair of RC is developed according to Miniguano et al.<sup>27</sup> The developed ECM is shown in Figure 1.  $V_{OC}$  is the open-circuit voltage.  $R_0$  is the internal resistance of the battery cells, and  $R_1$  and  $C_1$  are the parasitic resistor and capacitor, respectively. Using KVL, the terminal voltage of the battery can be written as follows:

$$V_t = V_{OC} - R_0 I - V_1, \quad (1)$$

$$V_1 = R_1 \left(1 - e^{-\frac{t}{R_1 C_1}}\right) I, \quad (2)$$

where  $V_t$  is the terminal voltage,  $I$  is the input current, and  $V_1$  is the voltage across the parasitic resistance ( $R_1$ ) and capacitance ( $C_1$ ).

RC values can be estimated in different SoCs and temperatures using the hybrid pulse power characterization (HPPC) test. This test determines the transient behaviors of a battery cell.<sup>23</sup> In this study, the HPPC test is executed for A123 Systems ANR26650M1-B LFP LIB cell, in which the cathode is  $\text{LiFePO}_4$ , at the temperature of 25°C and 35°C. The operating temperature range of this

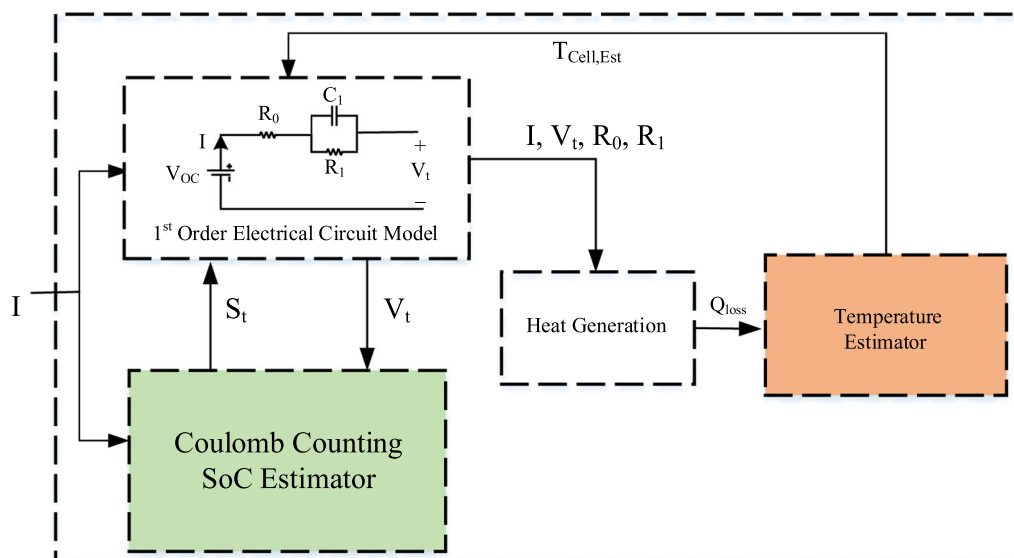


FIGURE 1 Electrothermal model of a battery cell.



battery cell is between  $-30^{\circ}\text{C}$  and  $55^{\circ}\text{C}$ ; however, the chosen temperatures of  $25^{\circ}\text{C}$  and  $35^{\circ}\text{C}$  reflect conditions in real-world scenarios while ensuring the avoidance of extremes that could impact battery health.<sup>28</sup> As such, the upper temperature can increase safety concerns of possible thermal runaway and accelerate aging due to the growth of solid-electrolyte interface (SEI) layers.<sup>29,30</sup> The HPPC test results of the battery cell's terminal voltage, current, and SoC at the temperature of  $35^{\circ}\text{C}$  are shown in Figure 2. In the HPPC test, the fully charged cell discharges after a pulse discharge current and a pulse charge current for 15 minutes and rests for an hour. These steps are repeated until the battery cell is discharged. The HPPC test results identify the battery cell's open-circuit voltage ( $V_{\text{OC}}$ ), internal resistance ( $R_0$ ), and the RC values employing the Optimization and Fitting Toolboxes in MATLAB environment for the full ranges of SoC and temperature. Figure 3 shows the battery cell parameters for the temperature of  $25^{\circ}\text{C}$  and  $35^{\circ}\text{C}$ . The terminal voltages are closely matched at both temperatures, yet,  $R_0$  increases when temperature increases. The rest of the RC values track the transient behavior of the cells based on the HPPC test.

## 2.2 | SoC estimation

Different SoC estimation methods are suggested in the literature<sup>7</sup> to improve accuracy. In this particular study, the emphasis is on cell balancing control rather than SoC estimation accuracy. Consequently, SoC values are considered inputs from the BMS and modeled employing the Coulomb counting method due to its

low implementation complexity and acceptable accuracy. The SoC of the cell is determined as follows:

$$S_t = S_{\text{ini},t_0} + \int_{\tau=t_0}^t \frac{I}{3600E_{\text{nom}}} d\tau, \quad (3)$$

where  $S_{\text{ini},t_0}$  and  $S_t$  are the initial SoC at  $t_0$  and the SoC of a battery cell at time  $t$ , respectively,<sup>31</sup> and  $I$  and  $E_{\text{nom}}$  are the cell's input current and nominal capacity, respectively. In the Coulomb counting method, the input current ( $I$ ), cell nominal capacity ( $E_{\text{nom}}$ ), and the initial SoC of the cell ( $S_{\text{ini},t_0}$ ) are determined as inputs to estimate the SoC. The estimated SoC is used as feedback to adjust battery cell parameters according to its estimated SoC level.

## 2.3 | Thermal model design

Depending on the application, battery thermal models can capture heat transfers from low to high accuracy levels. Refs. 32–35 present thermal models for different LIB chemistries in the automotive industry. The electrothermal battery cell model and its parameters are developed based on Refs. 32, 36, 37 Cylindrical LFP battery cells are considered for this study. The LFP cell parameters can be found in Table 1. According to Jaguemont et al.,<sup>32</sup> the energy balance equation capturing dynamic changes in each battery cell temperature is defined as follows:

$$mC_p \frac{dT_{\text{cell}}}{dt} = Q_{\text{loss}} - Q_{\text{conv}}, \quad (4)$$

where  $m$  is the cell mass,  $C_p$  is the specific heat of the cell,  $T_{\text{cell}}$  is the cell temperature,  $Q_{\text{loss}}$  is the internal heat

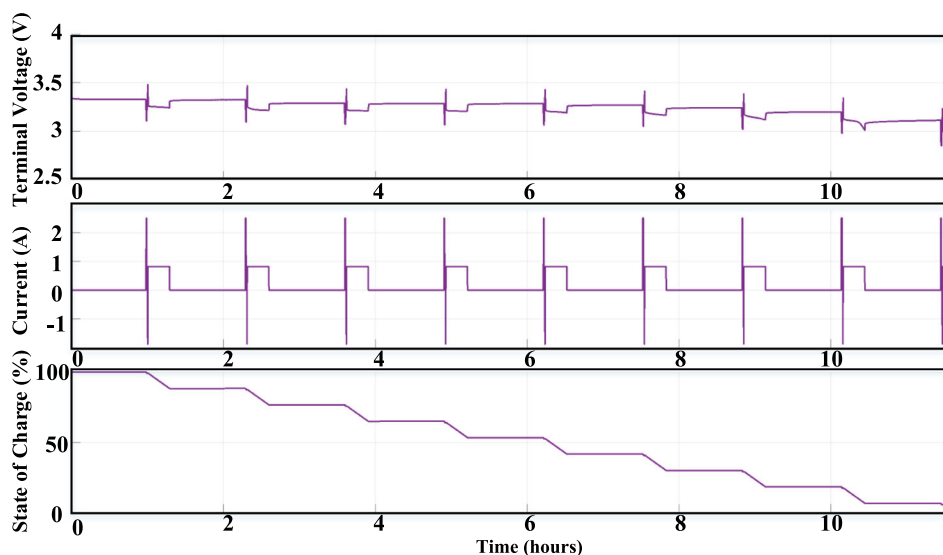


FIGURE 2 Hybrid pulse power characterization test results for the ANR26650M1-B lithium iron phosphate battery cell at  $35^{\circ}\text{C}$ .

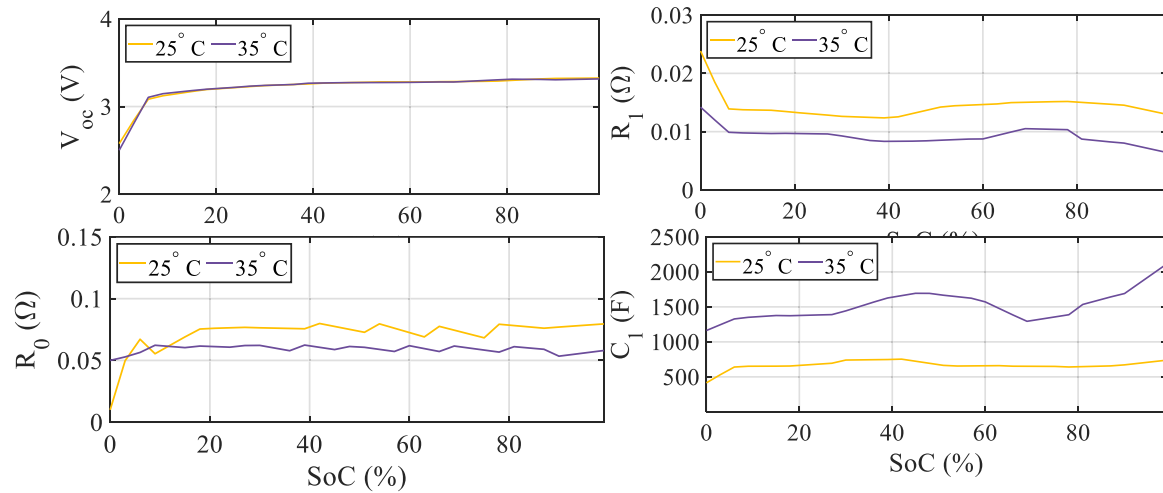


FIGURE 3 Open-circuit voltages and resistor-capacitor values for the full range of state of charges and temperature of 25°C and 35°C.

TABLE 1 Parameters of the lithium iron phosphate cylindrical battery cell.

Cell weight	$m$	73 g
Cell radius	$r$	13 mm
Cell height	$h$	65 mm
LFP-specific heat	$C_p$	1390 J/(Kg.K)
Heat transfer coefficient	$H$	10W/m <sup>2</sup> . K
Cell nominal energy	$E_{nom}$	2.5 Ah
Cell nominal terminal voltage	$V_t$	3.3 V

generation of the cell, and  $Q_{conv}$  is the convective heat transfer with the surrounding air. The conductive and radiation heat transfers are assumed negligible and are avoided for simplicity. The battery cell parameters are modeled as lumped parameters. The internal heat generation  $Q_{loss}$  is calculated using the electrical model of the battery cell from Section (2.1) as follows:

$$Q_{loss} = R_0 I^2 + R_1 I_1^2 = I(V_{OC} - V_t), \quad (5)$$

where  $I$  is the input current into the battery cell,  $V_{OC}$  is the open-circuit voltage,  $V_t$  is the terminal voltage of the battery cell,  $R_0$  is the internal resistance of the cell, and  $R_1$  and  $I_1$  are the parasitic resistance and its current, respectively. The internal and parasitic resistances are affected by both temperature and SoC of the cell. Finally, the convective heat transfer ( $Q_{conv}$ ) with the surrounding air is calculated based on Jaguemont et al.<sup>32</sup> as follows:

$$Q_{conv} = HA(T_a - T_{cell}), \quad (6)$$

where  $A$  is the area ( $m^2$ ),  $H$  is the convective heat transfer coefficient, and  $T_a$  is the ambient temperature.

Using Equations (4)–(6), cell temperatures can be estimated. Cell parameters are then updated according to the estimated temperature shown in Figure 1.

### 3 | CELL BALANCING CIRCUIT DESIGN

The design of the cell balancing circuit is tied to the selected cell balancing methods. The proposed C2P method refers to the transfer of power from individual cells to the battery pack, aiming to balance the states of all battery cells. The utilization of the C2P method is limited to the charging period of the battery pack. It can be noted that the method's key advantage of achieving balanced cell states without causing an increase in the average temperature due to limiting the charging power into the cells. Moreover, the simplicity of the circuit design is enhanced by its unidirectional nature when compared to bidirectional topologies. Among the various circuit designs, the flyback converter stands out as one of the most favored for implementing the C2P method. This design has several advantages such as compact size, cost-effectiveness, and high efficiency within the low to medium power range.<sup>16</sup> The flyback converter employs a coupled inductor to facilitate higher voltage ratio conversions and enables the provision of multiple outputs through multiple-output windings.<sup>15</sup> Both single-output winding and multiple-output windings flyback converters find application in BMS and cell balancing designs, each offering its own set of advantages and drawbacks.<sup>15–17</sup> The single-output winding flyback

converter per cell has a quicker balancing period compared to the multiple-output windings flyback converter. This speed advantage in the former approach is because all cells can engage in the balancing process simultaneously.<sup>16</sup> Figure 4 shows the flyback converter balancing circuit applied to cells in series in this study. The following section dives into the details of the design for the single-winding flyback converter used in the balancing circuit.

### 3.1 | Average modeling of flyback converter

The average model of the flyback converter is essential for this type of study due to the heavy computational

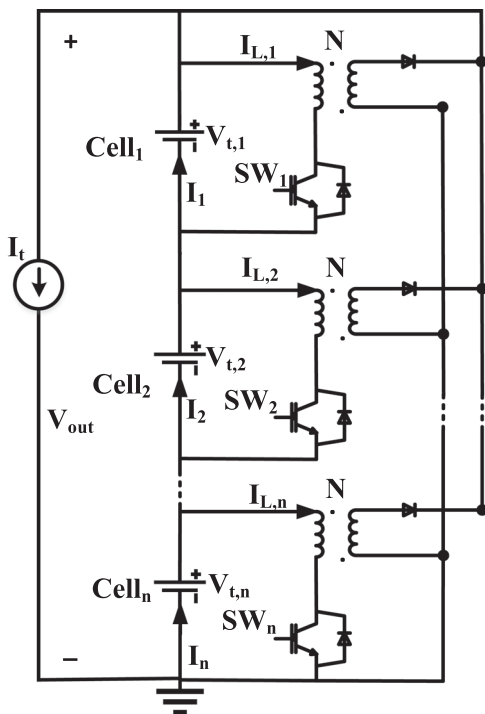


FIGURE 4 Flyback converters balancing circuit.

burden the switching has on simulation time. The design of the average model of the flyback converter for the DCM mode is discussed based on Akbarabadi et al.<sup>38</sup> In average modeling, the MOSFET switch and the diode of the flyback converter in Figure 5A are modeled as the variable current source ( $I_g$ ) and the variable voltage source ( $V_2$ ), respectively, in Figure 5B. Since the designed flyback converter is operating in DCM mode, the second duty cycle ( $D_2$ ) is required as follows:

$$D_2 = \min \left\{ \frac{2L f_{sw} I_g}{D_1 V_t} - D_1, (1 - D_1) \right\}, \quad (7)$$

where  $I_g$ ,  $f_{sw}$ ,  $L$ , and  $V_t$  are the average input balancing current, switching frequency, equivalent primary inductance, and input voltage, respectively.  $D_1$  is the duty cycle calculated by the PI current controller shown in Figure 6A so that the desired current  $I_g$  is provided. Calculating  $D_2$ , the average output voltage  $V_{out}$  and average input voltage ( $V_t$ ) are calculated from the primary side. The average input and output voltages can be written as follows:

$$V_1 = D_1 V_t, \quad (8)$$

$$V_2 = ND_2 V_{out}, \quad (9)$$

Using  $V_1$ ,  $V_2$  and inductance and resistance values (i.e.,  $L$  and  $R$ ),  $I_g$  can be computed using KVL from Figure 5.

### 3.2 | Flyback converter parameter design

Figure 5A shows the flyback converter switched-based model used to design the converter parameters and the PI controller. Flyback converters can operate in both continuous conduction mode (CCM) and DCM. The DCM releases all the stored energy in the flyback transformer inductor in each cycle. This release resets the magnetic flux to avoid electromagnetic saturation

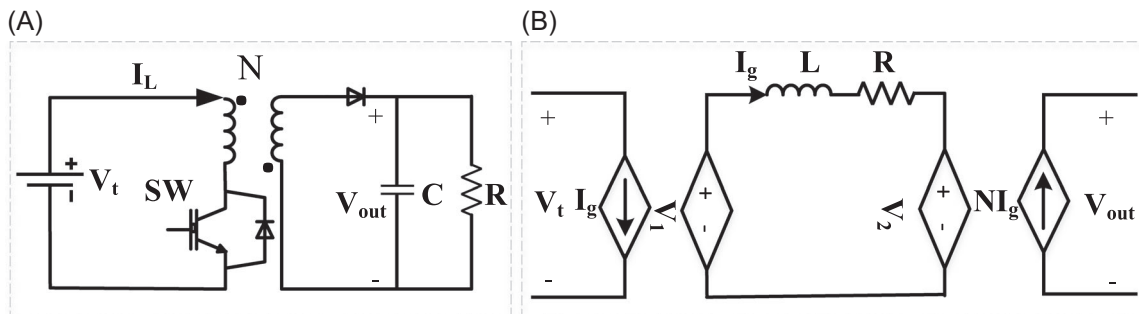
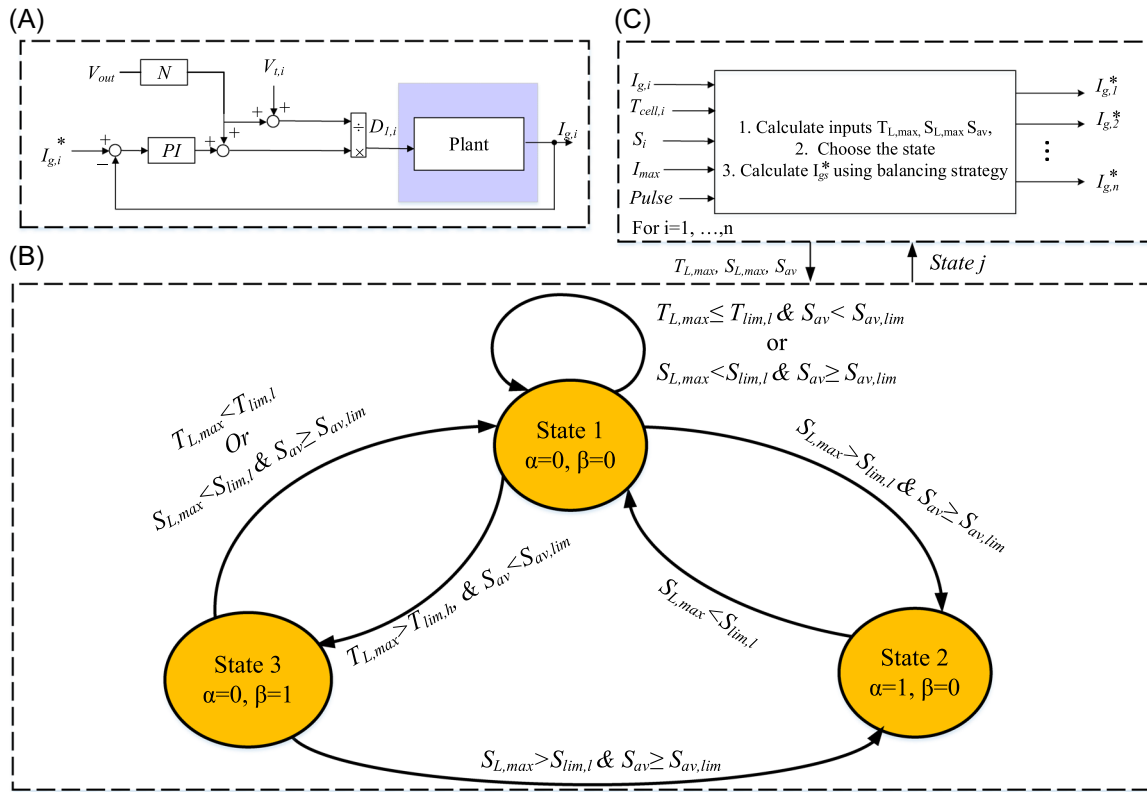


FIGURE 5 (A) Flyback converter switched-based model and (B) flyback converter average model.





**FIGURE 6** Proposed thermal and state of charge-based balancing control design, (A) inner current loop controller of the flyback converter  $i$ , (B) finite-state machine-based controller, and (C) balancing strategy controller inner current controller design.

and subsequently improves the efficiency and stability of the power converter.<sup>17,39</sup> Therefore, the DCM is selected for this study. The maximum primary inductance to design a DCM flyback converter can be calculated from the stored energy in the primary inductor and the voltage over the primary inductor when the switch is on. The equation can be written as follows:

$$L \leq \frac{D_{1,\max}^2 V_{t,\min}}{2f_{\text{sw}} I_{g,\max}}, \quad (10)$$

where  $D_{1,\max}$  is the maximum duty cycle,  $\mu$  is the efficiency,  $V_{t,\min}$  is the minimum input voltage (i.e., the minimum battery cell terminal voltage),  $f_{\text{sw}}$  is the switching frequency, and  $P_o$  is the output power. The worst case is when the converter operates with the minimum terminal voltage and the maximum duty cycle to ensure the DCM operation of the flyback converter. Additionally, the turning ratio  $n$  is required which is computed from

$$N = \frac{V_t}{V_{\text{out}}}. \quad (11)$$

Finally, the capacitance value is designed to mitigate the output voltage ( $V_{\text{out}}$ ) ripple. The flyback converter parameters are listed in Table 2.

**TABLE 2** Flyback power converter parameters.

Input voltage	$V_t$	2.5–3.6 V
Output voltage	$V_{\text{out}}$	10–14.4 V
Maximum current	$I_{g,\max}$	5 A
Switching frequency	$f_{\text{sw}}$	50 kHz
Inductance	$L$	1 $\mu\text{H}$
Turning ratio	$N$	0.25

## 4 | CELL BALANCING CONTROL DESIGN

In this section, the control design and balancing strategies are discussed in detail.

### 4.1 | Inner current controller design

Each flyback converter is operating independently using its inner current controller. The design of the current controller for flyback converters is based on the average model of the flyback converter derived from Erickson.<sup>40</sup> The relation between transformer inductance current ( $I_L$ )

and the voltage across the inductance ( $V_L$ ) can be written as the transfer function which is

$$G_{I_L, V_L} = \frac{I_L(s)}{V_L(s)} = \frac{1}{Ls + R}, \quad (12)$$

where  $L$  and  $R$  are the transformer equivalent inductance and resistance, respectively. Three operating stages for the DCM flyback converter are (1) the switch (SW) is on ( $D_1 T_{SW}$ ), (2) the switch is off ( $D_2 T_{SW}$ ), and (3) both switch and diode are off ( $1 - D_1 - D_2$ ).  $D_1$  represents the first duty cycle,  $D_2$  is the second duty cycle, and  $T_{SW}$  is the time period ( $T_{SW} = \frac{1}{f_{sw}}$ ). Using KVL for these two stages, the relation between  $V_L$  and voltages ( $V_i$  and  $V_{out}$ ) can be written as follows:

$$\text{Stage 1, } V_L(t) = V_i(t)$$

$$\text{Stage 2, } V_L(t) = -NV_{out}(t).$$

$$\text{Stage 3, } V_L(t) = 0$$

Using KVL in Figure 5B, the average of  $V_L(t)$  in one switching cycle ( $T_{sw}$ ) is

$$V_L(t) = D_1(t)V_i(t) - (D_2(t))NV_{out}(t). \quad (13)$$

Using the above equation, the duty cycle  $D_1(t)$  for the converter can be derived as follows:

$$D_1(t) = \frac{D_2 NV_{out}(t) + V_L(t)}{V_i(t)}, \quad (14)$$

$V_L(t)$  is the output of the PI controller to regulate the  $I_g$  to  $I_g^*$ . The state space model of the power converter is required to design the PI current controller for the cell balancing flyback converter. The state space model of the flyback converter in the DCM is developed based on its average model and can be written as follows:

$$\begin{bmatrix} \frac{dI_L(t)}{dt} \\ \frac{dV_{out}(t)}{dt} \end{bmatrix} = \begin{bmatrix} 0 & \frac{-ND_2(t)}{L} \\ \frac{ND_2(t)}{C} & \frac{-1}{RC} \end{bmatrix} \begin{bmatrix} I_L(t) \\ V_{out}(t) \end{bmatrix} + \begin{bmatrix} \frac{D_1(t)}{L} \\ 0 \end{bmatrix} V_i(t), \quad (15)$$

$$I_g = [D_1 \quad 0] \begin{bmatrix} I_L \\ V_{out} \end{bmatrix}, \quad (16)$$

where  $I_L$  is the current that goes into the inductance ( $L$ ). Using the state space Equations (15) and (16), the transfer function between  $V_i$  and  $I_g$  is calculated as follows:

$$H(s) = C(sI - A)^{-1}B + D = \frac{\frac{D_1^2}{L} \left( s + \frac{1}{RC} \right)}{s \left( s + \frac{1}{RC} \right) + \frac{n^2 D_2^2}{LC}}. \quad (17)$$

This transfer function represents the plant model. Deploying the transfer function in Equation (17), the PI controller is designed using PI tuning toolbox. Figure 6A shows the schematic of the inner current controller of the flyback converter for the cell balancing of cell  $i$ .

## 4.2 | Proposed balancing controller and balancing strategy

The simultaneous temperature and SoC balancing can be formulated as an optimization problem. To achieve that, we begin by calculating the average values of battery cell states. The average SoC is  $S_{av} = \frac{1}{n} \sum_{i=1}^n S_i$ , and the average temperature is  $T_{av} = \frac{1}{n} \sum_{i=1}^n T_i$ , where  $n$  is the number of series cells. Using the average states, the SoC error vector for  $n$  series cells can be written as

$$\begin{bmatrix} S(I_1, E_{nom,1})_{L,1} \\ \vdots \\ S(I_n, E_{nom,n})_{L,n} \end{bmatrix} = \begin{bmatrix} S(I_1, E_{nom,1})_1 \\ \vdots \\ S(I_n, E_{nom,n})_n \end{bmatrix} - S_{av} \mathbf{1}_{n \times 1}. \quad (18)$$

And the temperature error vector for  $n$  series cells as

$$\begin{bmatrix} T(I_1)_{L,1} \\ \vdots \\ T(I_n)_{L,n} \end{bmatrix} = \begin{bmatrix} T(I_1)_1 \\ \vdots \\ T(I_n)_n \end{bmatrix} - T_{av} \mathbf{1}_{N \times 1}. \quad (19)$$

The error vectors are required to define the optimization problem. The objectives of the optimization problem are temperature and SoC balancing. In this study, the simultaneous balancing of temperature and SoC is redefined based on the battery pack needs. Therefore, the first objective is to ensure balanced SoCs by the end of charge, and the second objective is the temperature balancing to mitigate the nonuniform distribution of the temperature among cells. Also, the balancing should be achieved without increasing the average temperature of cells compared to that when no balancing design operates since increasing the temperature contributes to additional cell aging. This feature is satisfied by employing the C2P balancing design during the charging period which decreases the charging current of the unbalanced battery cells. Taking the two objectives into account, the optimization problem for temperature and SoC balancing can be expressed as a minimization of a linear combination of the two objectives in a single cost function, as outlined below.

$$\min_{I_i} \alpha \|S(I_i, E_{nom,i})_{L,i,t_{end}}\|_{\infty} + \beta \int_0^{t_{end}} \|T(I_i)_{L,i}\|_{\infty} d\tau, \quad (20)$$

$$\text{for } i = 1, \dots, n, \quad (21)$$

$$\text{s.t. } I_t - I_{g,i} \leq I_i \leq I_t, \quad i = 1, 2, \dots, n, \quad (22)$$

$$S_{\min} \leq S_i \leq S_{\max}, \quad i = 1, 2, \dots, n, \quad (23)$$

where  $t_{\text{end}}$  is the end of the charging time and  $\alpha$  and  $\beta$  are tradeoff weights, which show the relative importance of each objective during the charging period. These two weights are chosen in a way that  $\alpha + \beta = 1$  to achieve the tradeoff between SoC and temperature balancing. To solve this optimization problem, a finite-state machine-based approach is proposed to avoid complexity and heavy computations compared to literature such as which is not favorable for online BMS designs. In the following section, first, the proposed control design is described, and then, the proposed balancing strategy is presented.

#### 4.2.1 | Proposed finite-state machine-based control design

In the proposed finite-state machine-based control design, three states are defined. Each state has its balancing strategy. Depending on the operating states defined based on the tradeoff weight, the proposed controller decides on the balancing approach. These states depend on the SoC and temperature criteria and by changing the  $\alpha$  and  $\beta$  values. The operating state is decided based on the limiting criteria for the maximum SoC derivation ( $S_{L,\max}$ ), the maximum temperature derivation ( $T_{L,\max}$ ), and the average SoC ( $S_{av}$ ) at each sampling instant ( $k$ ). The limiting criteria for  $S_{L,\max}$  are the SoC limit ( $S_{\text{lim},l}$ ). The limiting criteria for  $T_{L,\max}$  are the lower bound limit ( $T_{\text{lim},l}$ ) and the upper bound limit ( $T_{\text{lim},h}$ ). The criteria for  $S_{av}$  is the average SoC limit ( $S_{av,\text{lim}}$ ). The  $S_{\text{lim},l}$ ,  $T_{\text{lim},l}$ , and  $T_{\text{lim},h}$  values are chosen as 0.1%, 0.5°C, and 0.6°C respectively, to avoid fast and unnecessary state changing, unlike the other optimization solution in Altaf and Egardt.<sup>20</sup> The value of  $S_{av,\text{lim}}$  is dependent on the maximum charging current ( $I_{t,\max}$ ) and  $S_{L,\max}$  to ensure the SoCs are balanced before reaching the 80% charging level.  $S_{av,\text{lim}}$  is defined as

$$S_{av,\text{lim}} = \begin{cases} 80\%, & 0 < 80\% - \gamma S_{L,\max} \frac{I_t}{I_{t,\max}} \\ 0\%, & 80\% - \gamma S_{L,\max} \frac{I_t}{I_{t,\max}} \leq 0, \end{cases} \quad (24)$$

where  $\gamma$  is the maximum change in the  $S_{av}$  to balance the  $S_{L,\max}$  of 1% which is calculated to be 3%,  $I_t$  is the charging current, and  $I_{t,\max}$  is the maximum charging current of battery cells in series, which is 10 A for the

studied cells. Two operating factors,  $\alpha$  and  $\beta$  are two binary factors. If  $\alpha$  is 1, the SoC balancing is active and if it is zero, the SoC balancing is inactive. Similarly, for  $\beta$ , if it sets at 1, the temperature balancing is active and if it is zero, the thermal balancing is inactive. Three states are defined for this design as follows.

- **State 1:** If both temperature differences and the SoC differences are within the defined criteria or the SoCs are balanced and the average SoC is more than  $S_{av,\text{lim}}$  for state 1 as shown in Figure 6C, State 1 happens. In this state, two operating factors  $\alpha$  and  $\beta$  are both zeros in this state meaning balancing circuits are off.
- **State 2:** When the defined criteria shown in Figure 6C for State 2 are met, the state operating changes to State 2. In this state, the priority is to balance SoCs. State 2 stays until  $S_{L,\max}$  is less than or equal to the minimum allowed SoC imbalance ( $S_{\text{lim},l}$ ) and  $S_{av}$  is greater than  $S_{av,\text{lim}}$ . Operating factor  $\alpha$  is set at one, and  $\beta$  is set at zero in the state.
- **State 3:** According to the defined criteria in Figure 6C, in State 3, the priority is to balance temperatures. This state happens when  $T_{L,\max}$  reaches its upper bound limit ( $T_{\text{lim},h}$ ). State 3 stays until  $S_{av}$  is smaller than  $S_{av,\text{lim}}$  or  $T_{L,\max}$  is less than  $T_{\text{lim},l}$ , meaning cell temperatures are balanced. Therefore, operating factors  $\alpha$  and  $\beta$  are set at zero and one, respectively.

Figure 6B,C show the state machine criteria and the balancing controller for temperature and SoC balancing, respectively. As can be observed in Figure 6B, the balancing controller calculates the reference current for the inner current control loop for each battery cell. The sampling period for the state machine is supposed to be longer than the inner current control loop's sampling period to ensure the stability of the control design. In this study, the sampling time  $k$  happens every 1 s due to slower dynamic changes in thermal modeling compared to ones in electrical modeling. In other words, the temperature estimator is designed to update temperature and heat transfer values every 1 s.

#### 4.2.2 | Proposed SoC and temperature balancing strategy

A proposed balancing strategy is suggested to balance either SoCs or temperatures. The proposed strategy balances battery cells' parameters without requiring them to solve complicated and computationally heavy optimization problems. In Figure 7, the proposed strategy is shown for SoC balancing. The proposed strategy calculates the reference cell balancing current for each

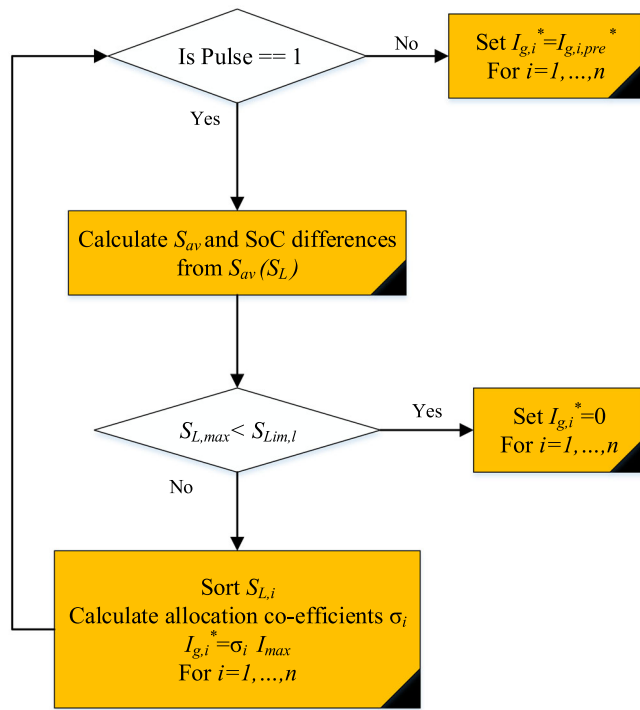


FIGURE 7 Proposed state of charge (SoC)-based balancing strategy.

cell according to their SoCs at each time step ( $k$ ) for the next time step ( $k + 1$ ) using a pulse with the frequency of 1000Hz. The proposed strategy for SoC balancing is discussed as follows.

- **Step 1:** At time step  $k$ , the SoC ( $S_i$ ), the charging current ( $I_t$ ), and the maximum allowed cell balancing current of each cell ( $I_{cb,max}$ ) are received. If  $I_t$  is less than the  $I_{cb,max}$ , then the maximum cell balancing current ( $I_{max}$ ) is set equal to  $I_t$ , if not  $I_{max}$  equals  $I_{cb,max}$ .
- **Step 2:** The average SoC ( $S_{av}$ ) and the SoCs deviations ( $S_{L,i}$ ) from  $S_{av}$  are calculated. If the maximum SoC deviation ( $S_{L,max} = \|S_L\|_\infty$ ) among all cells is less than  $S_{lim,l}$  (i.e., 0.1%), no balancing is required (i.e.,  $I_{g,i} = 0$  for  $i = 1, \dots, n$ ). If not, the algorithm calculates the allocation coefficients  $\sigma_i$  based on the  $S_{L,i}$  as

$$\begin{bmatrix} \sigma_1 \\ \vdots \\ \sigma_n \end{bmatrix} = \begin{bmatrix} S_{L,1} \\ \vdots \\ S_{L,n} \end{bmatrix} - S_{L,\min} \mathbf{1}_{n \times 1}, \quad (25)$$

where  $S_{L,\min}$  is the minimum of  $S_{L,i}$  when  $i = 1, \dots, n$  and  $\mathbf{1}_{n \times 1}$  is a matrix of ones with the size of  $n \times 1$ .

- **Step 3:** Go back to step 1 for the next time step  $k + 1$ .

Similar steps are followed to calculate  $\sigma$  coefficients for the temperature balancing strategy. For charging, the cell

with the highest temperature requires to discharge with the highest balancing current to mitigate the input current into the cell. Subsequently, step 2, during the temperature balancing, is to calculate the  $T_{av}$  and the error vector of  $T_L$ . And, calculating the allocation coefficients  $\sigma_i$  as follows:

$$\begin{bmatrix} \sigma_1 \\ \vdots \\ \sigma_n \end{bmatrix} = \begin{bmatrix} T_{L,1} \\ \vdots \\ T_{L,n} \end{bmatrix} - T_{L,\min} \mathbf{1}_{n \times 1}, \quad (26)$$

where  $T_{L,\min}$  is the minimum temperature among all the  $T_i$ s for  $i = 1, \dots, n$ .

## 5 | SIMULATION RESULTS

In this section, case studies are developed to study the performance of the proposed control design and balancing strategy. Four battery cell electrothermal models with their flyback converter balancing circuit averaged model in series are simulated in Matlab/Simulink. The battery cell parameters are listed in Table 1. The battery cell ECM parameters vary depending on their SoC levels and temperatures shown in Figure 3. Parameters of flyback converters are listed in Table 2. The ambient temperature is set at 25°C. Additionally, the effect of the thermal management system in the BMS is neglected to focus on the effects of the balancing system on battery cells' SoCs and temperatures. Several case studies evaluate the performance of the proposed control design and balancing approach in the following subsections.

### 5.1 | Proposed SoC balancing performance in comparison with a conventional method

In this case, the proposed SoC balancing strategy is compared with the method suggested in Brandis et al.<sup>41</sup> on four cells in series with the same ambient and internal temperatures and with different initial SoCs. The conventional method slows down the charging of a cell with the highest SoC. Cells' SoCs have a 1% difference from each other at the start and the battery cells are charged with 5 A current. The simulation results show the cells' input currents, SoCs, and temperatures for (a) the proposed method and (b) the conventional method in Figure 8. The proposed SoC balancing allocates the input currents ( $I_i$ ) by setting the reference currents ( $I_{g,i}^*$ ) for balancing circuits. The battery cell SoC error decreases to less than 0.1% after 49 s, while it reaches less than 0.1% after 94 s in the conventional method. Additionally, the SoC balancing strategy causes up to 0.75°C temperature

imbalance among cells by the end of the SoC balancing process in both cases.

## 5.2 | Proposed temperature balancing performance

In this case study, the proposed temperature balancing strategy without the SoC balancing is implemented on the four cells in series with different initial internal temperatures and the same ambient temperatures and initial SoCs. The simulation results show the SoCs and temperatures of the battery cells for 200 s while each cell has a 1°C difference initially. In Figure 9, battery cells' SoCs ( $S_i$ ), temperatures ( $T_i$ ), and input currents ( $I_i$ ) for  $i = 1, \dots, 4$  are shown. The temperature balancing time is almost twice longer than 100 s compared to the balancing time for the proposed SoC balancing strategy. The maximum cell temperature differences from the average temperature ( $T_{L,max}$ ) is less than 0.5°C and caused more than 3% SoC imbalance from the average SoC.

## 5.3 | Proposed finite-state control design performance with constant current charging

The proposed finite-state machine-based balancing strategy is shown in this case study. Figure 10 shows the SoCs

( $S_i$ ), temperatures ( $T_i$ ), and cell voltages ( $V_{t,i}$ ) for the proposed controller. The proposed controller balances battery cells' temperature during the charging process and balances the SoC imbalances before the average SoC ( $S_{av}$ ) reaches 80% charge level while without any balancing control, temperatures are unbalanced and cell

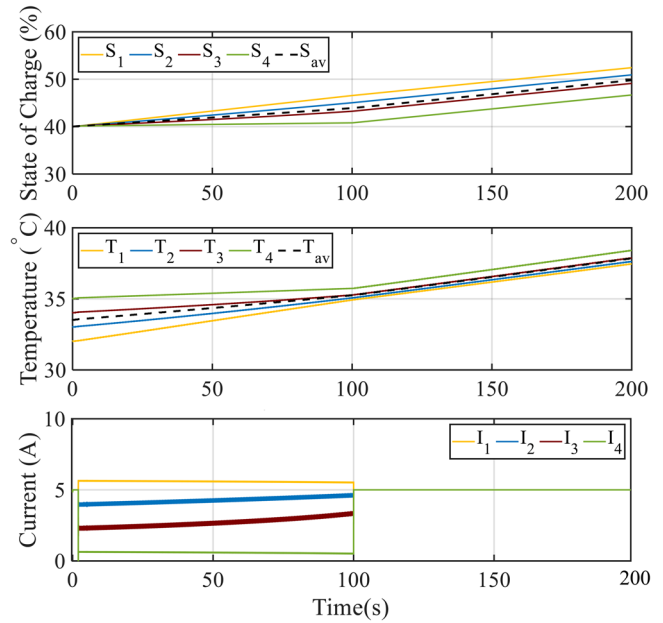


FIGURE 9 Results of input currents ( $I_i$ ), state of charges (SoCs) ( $S_i$ ), and temperatures ( $T_i$ ) of the cell  $i$  for  $i = 1, \dots, 4$ .

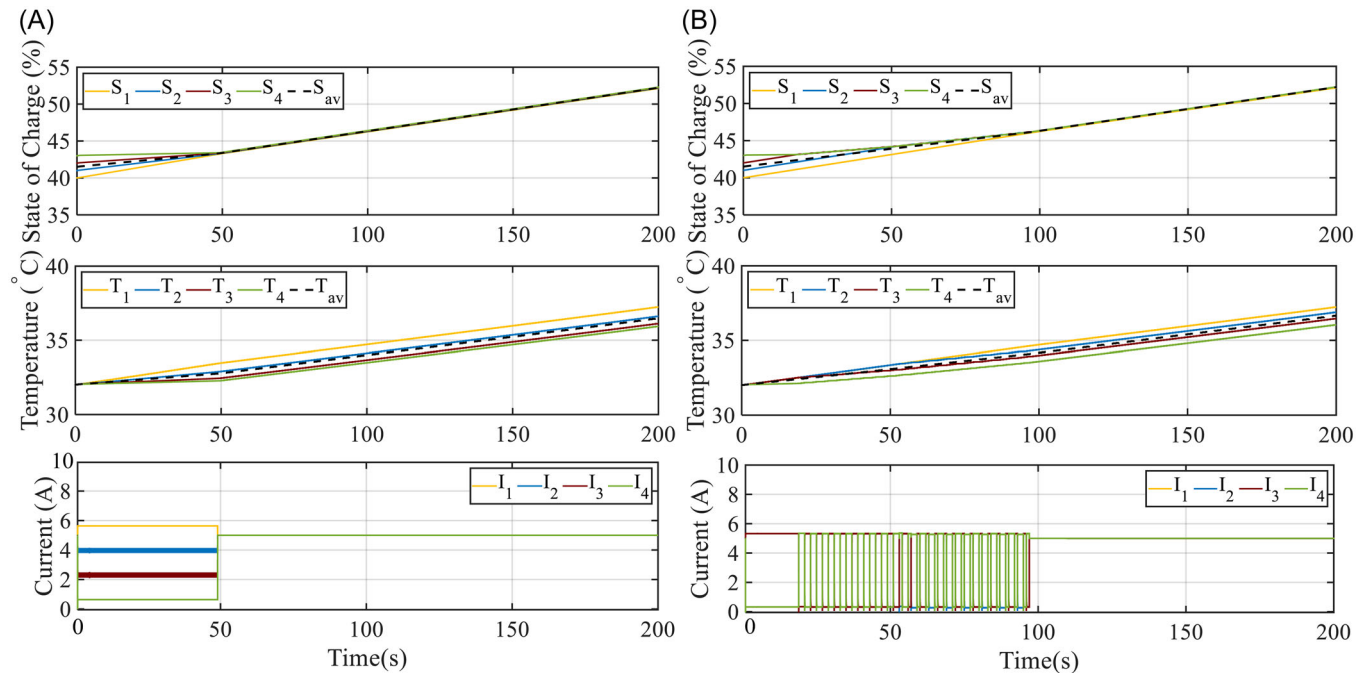


FIGURE 8 Results of input currents ( $I_i$ ), state of charges (SoCs) ( $S_i$ ), and temperatures ( $T_i$ ) of the cell  $i$  for  $i = 1, \dots, 4$  for (A) the proposed balancing strategy and (B) the conventional method.



1 with the highest SoC ( $S_1$ ) limits the charging capacity to avoid overcharging of cell 1. Additionally, in Figure 10, changes in the operating states cause different cell terminal voltages ( $V_{t,i}$ ) since the input current for each cell is different depending on the operating state. The operating state of the proposed controller is shown in Figure 11. In the beginning, the proposed controller operates on state 3 to balance temperature. After

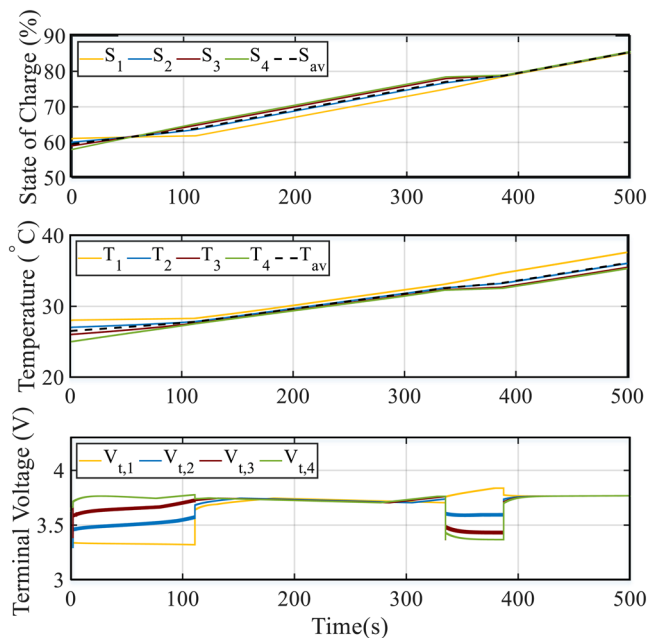


FIGURE 10 Simulation results of state of charges (SoCs) ( $S_i$ ), temperatures ( $T_i$ ), and voltages ( $V_{t,i}$ ) using the proposed finite-state machine-based balancing strategy.

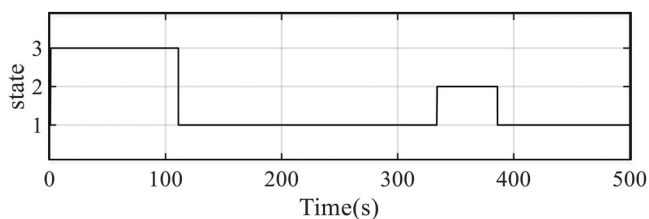


FIGURE 11 State changes between states 1, 2, and 3 when using the proposed finite-state machine-based balancing strategy.

TABLE 3 Comparison between battery cells' temperatures and state-of-charges (SoCs) with different types of control modes.

Type of control	No control	SoC-based control	Temperature-based control	Finite-state machine-based control
$S_{L,max}$ for $S_{av} > 80\%$	1.5%	0.1%	2.1774%	0.1%
Maximum root mean squared error for $T$	1.7830°C	1.2836°C	0.6512°C	0.9670°C
Charging time from 60% to 80%	349.5 s	365 s	386.2 s	407.6 s

balancing temperatures, when  $S_{av}$  reaches  $S_{av,lim}$ , state 2 balances SoCs to ensure balanced SoCs before reaching the 80% charging limit. The proposed control design avoids fast state changes by defining limits,  $T_{lim,h}$  and  $T_{lim,l}$  for the temperatures of cells. To compare the effectiveness of the proposed control design with the other approaches, the maximum root mean squared error (RMSE) of  $T_i$  is calculated for each method. The RMSE is defined based on Chai and Draxler<sup>42</sup> as  $\sqrt{\frac{1}{t_n} \sum_{i=1}^{t_n} \|T_{L,i}\|_{\infty}^2}$ , where  $t_n$  is the simulation period. Table 3 compares the  $S_{L,max}$  values (when  $S_{av}$  is greater than 80%), the maximum RMSE of  $T_i$ s, and the charging time from 60% to 80% for (1) no balancing control, (2) only proposed SoC-based balancing control, (3) only proposed temperature-based balancing control, and (4) the proposed finite-state machine-based control operates in the same operating condition as Figure 10. The SoC-based control balances the SoCs, yet it has a large RMSE. The temperature-based control has the smallest RMSE compared to other methods, yet the SoC is not balanced. The  $S_{L,max}$  for the proposed finite-state machine-based control is at 0.1%, while it has a lower RMSE value compared to SoC-based control and no control strategy; yet, it has a longer balancing time compared to other methods. The proposed finite-state machine-based control improves the temperature balancing between cells during the charge without compromising the SoC balancing requirements which maximize the charging capacity.

#### 5.4 | Proposed finite-state control design performance with 10 cells in series

In this case study, the effectiveness of the proposed control design is assessed using a configuration of 10 series-connected cells. This configuration is intentionally set up to represent the most extreme scenario of SoC and temperature imbalances. Meaning the cell with the highest SoC has the lowest temperature and vice versa; consequently, the temperature balancing contributes to more SoC imbalance. As shown in Figure 12, initially,

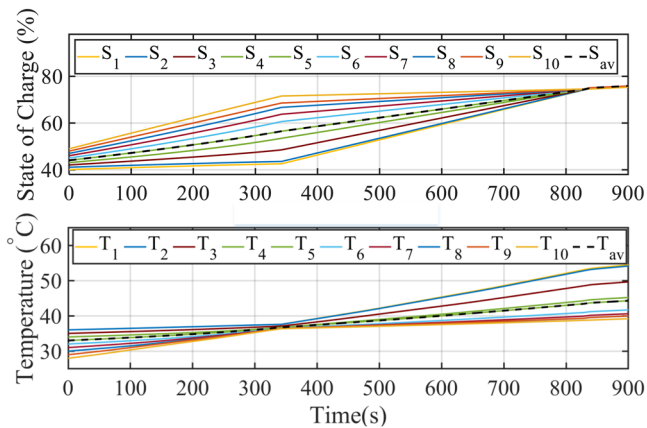


**FIGURE 12** Simulation results of state of charges ( $S_i$ ) and temperatures ( $T_i$ ) for the proposed finite-state machine-based balancing strategy with 10 series cells.

there are 9% SoC imbalances among the cells with maximum and minimum SoC and 9°C temperature imbalances between the cell with the highest temperature and the cell with the lowest temperature. The results for the temperature and SoCs in Figure 2 show that the control design balances the temperature during the charging until 345 s and then changes the operating mode to SoC balancing to ensure balanced SoCs before the average SoC reaches 80% charge. It should be noted that the maximum temperature reaches 54.45°C due to the lack of a thermal management system that mitigates the overall temperature of the battery pack.

## 6 | CONCLUSION

This study introduces an innovative finite-state machine-based control design that utilizes active balancing circuits (i.e., flyback converters) within the BMS to address two crucial objectives: achieving balanced SoCs and mitigating temperature imbalances. The proposed controller tackles the different battery cell aging in a battery pack using temperature balancing during the charging period and maximizes the energy capacity of a battery pack using SoC balancing closer to the end of charging process. Furthermore, the finite-state machine-based control design has the advantage of being more computationally efficient compared to optimization-based solvers due to its simplicity. The proposed control design is combined with the proposed balancing strategy which allocates currents of balancing circuits to balance either SoCs or temperatures. The results show the proposed balancing strategy has superior performance compared to the conventional method with regard to balancing speed. Finally, the results show that SoCs can balance faster compared to the temperatures due to slower heat transfer dynamics. This

observation indicates that integrating temperature balancing into the SoC balancing circuit could mitigate temperature imbalances among battery cells without interrupting the SoC balancing.

## ACKNOWLEDGMENTS

This work was supported in part by the Hydro-Quebec Center of Excellence in Transportation Electrification and Energy Storage through the Smart BMS Initiative and Mitacs under Award IT26874. Asal Zabetian-Hosseini and Benoit Boulet are with the Electrical and Computer Engineering Department, at McGill University, Montreal QC Canada. Amin Ghazanfari is with the Hydro-Quebec Center of Excellence in Transportation Electrification and Energy Storage, Montreal QC H2Z 1A4, Canada.

## CONFLICT OF INTEREST STATEMENT

The authors declare no conflict of interest.

## DATA AVAILABILITY STATEMENT

The battery cell test data are provided by the Hydro-Québec, Center of Excellence, and the authors elect to not share data.

## ORCID

Asal Zabetian-Hosseini  <http://orcid.org/0000-0002-5766-0398>

## REFERENCES

- Hadouchi M, Koketsu T, Hu Z, Ma J. The origin of fast-charging lithium iron phosphate for batteries. *Battery Energy*. 2022;1(1):20210010.
- Altaf F, Johannesson L, Egardt B. Simultaneous thermal and state-of-charge balancing of batteries: a review. *Proceeding of the 2014 IEEE Vehicular Power and Propulsion Conference (VPPC)*. Coimbra, Portugal; 2014:1-7.
- Paul S, Diegelmann C, Kabza H, Tillmetz W. Analysis of aging inhomogeneities in lithium-ion battery systems. *J Power Sources*. 2013;239(0378-7753):642-650.
- Chen L, Wu H, Ai X, Cao Y, Chen Z. Toward wide-temperature electrolyte for lithium-ion batteries. *Battery Energy*. 2022;1(2):20210006.
- Rumpf K, Naumann M, Jossen A. Experimental investigation of parametric cell-to-cell variation and correlation based on 1100 commercial lithium-ion cells. *J Energy Storage*. 2017;14(2352-152X):224-243.
- Schindler M, Sturm J, Ludwig S, Schmitt J, Jossen A. Evolution of initial cell-to-cell variations during a three-year production cycle. *eTransportation*. 2021;8(2590-1168):100102.
- Naguib M, Kollmeyer P, Emadi A. Lithium-ion battery pack robust state of charge estimation, cell inconsistency, and balancing: review. *IEEE Access*. 2021;9:50570-50582.
- Yildirim B, Elgendy M, Smith A, Pickert V. Evaluation and comparison of battery cell balancing methods. *Proceeding of the IEEE PES Innovative Smart Grid Technologies, Europe*. Bucharest, Romania; 2019:1-5.

9. Ghaeminezhad N, Ouyang Q, Hu X, Xu G, Wang Z. Active cell equalization topologies analysis for battery packs: a systematic review. *IEEE Trans Power Electron.* 2021;36:9119-9135.
10. Leng F, Ming Tan C, Pecht M. Effect of Temperature on the Aging rate of Li Ion Battery Operating above Room Temperature. *Sci Rep.* 2015;5:12967.
11. Kremer P, Cigarini F, Göhlich D, Park S. Active cell balancing for life cycle extension of lithium-ion batteries under thermal gradient. *Proceeding of the 2021 IEEE/ACM International Symposium on Low Power Electronics and Design (ISLPED)*. Boston, MA, USA; 2021:1-6.
12. Omariba ZB, Zhang L, Sun D. Review of battery cell balancing methodologies for optimizing battery pack performance in electric vehicles. *IEEE Access.* 2019;7:129335-129352.
13. Evzelman M, Ur Rehman MM, Hathaway K, Zane R, Costinett D, Maksimovic D. Active balancing system for electric vehicles with incorporated low-voltage bus. *IEEE Trans Power Electron.* 2016;31:7887-7895.
14. Imtiaz AM, Khan FH, Kamath H. A low-cost time shared cell balancing technique for future lithium-ion battery storage system featuring regenerative energy distribution. *Proceeding of the 2011 Twenty-Sixth Annual IEEE Applied Power Electronics Conference and Exposition (APEC)*. Fort Worth, TX, USA; 2011:792-799.
15. Imtiaz AM, Khan FH. "Time shared flyback converter" based regenerative cell balancing technique for series connected li-ion battery strings. *IEEE Trans Power Electron.* 2013;28:5960-5975.
16. Einhorn M, Roessler W, Fleig J. Improved performance of serially connected li-ion batteries with active cell balancing in electric vehicles. *IEEE Trans Veh Technol.* 2011;60:2448-2457.
17. Kumar A, Bhat AH, Agarwal P. Comparative analysis of dual active bridge isolated DC to DC converter with flyback converters for bidirectional energy transfer. *Proceeding of the 2017 Recent Developments in Control, Automation & Power Engineering (RDCAPE)*. Noida, India; 2017:382-387.
18. Wu F, Yi X, Gao F. Thermal balance control of lithium-ion battery packs based on bi-directional flyback converter. *Proceeding of the 2021 IEEE 1st International Power Electronics and Application Symposium (PEAS)*. Shanghai, China; 2021:1-4.
19. Guo X, Geng J, Liu Z, Xu X, Cao W. A flyback converter-based hybrid balancing method for series-connected battery pack in electric vehicles. *IEEE Trans Veh Technol.* 2021;70:6626-6635.
20. Altaf F, Egardt B. Comparative analysis of unipolar and bipolar control of modular battery for thermal and state-of-charge balancing. *IEEE Trans Veh Technol.* 2017;66:2927-2941.
21. Altaf F, Egardt B, Johannesson Mardh L. Load management of modular battery using model predictive control: thermal and state-of-charge balancing. *IEEE Trans Control Syst Technol.* 2017;25:47-62.
22. Li Y, Han Y. A new perspective on battery cell balancing: thermal balancing and relative temperature control. *Proceeding of the 2016 IEEE Energy Conversion Congress and Exposition (ECCE)*. Milwaukee, WI, USA; 2016:1-5.
23. Fotouhi A, Auger DJ, Propp K, Longo S. Accuracy versus simplicity in online battery model identification. *IEEE Trans Syst Man Cybern Syst.* 2018;48:195-206.
24. Yujie W, Jiaqiang T, Zhendong S, et al. A comprehensive review of battery modeling and state estimation approaches for advanced battery management systems. *Renew Sust Energy Rev.* 2020;131(1364-0321):110015.
25. Fuller TF, Doyle M, Newman J. Simulation and optimization of the dual lithium ion insertion cell. *J Electrochem Soc.* 1994;141:1-10.
26. Zhang C, Allafi W, Dinh Q, Ascencio P, Marco J. Online estimation of battery equivalent circuit model parameters and state of charge using decoupled least squares technique. *Energy.* 2018;142(0360-5442):678-688.
27. Miniguano H, Barrado A, Lazaro A, Zumel P, Fernandez C. General parameter identification procedure and comparative study of li-ion battery models. *IEEE Trans Veh Technol.* 2020;69:235-245.
28. Lu Z, Yu XL, Wei LC, et al. A comprehensive experimental study on temperature-dependent performance of lithium-ion battery. *Appl Therm Eng.* 2019;158:113800.
29. Zu C, Yu H, Li H. Enabling the thermal stability of solid electrolyte interphase in li-ion battery. *InfoMat.* 2021;3(6):648-661.
30. Qin M, Zeng Z, Cheng S, Xie J. Challenges and strategies of formulating low-temperature electrolytes in lithium-ion batteries. *Interdiscipl Mater.* 2023;2(2):308-336.
31. Jeong Y, Cho Y-K, Ahn J-H, Ryu S-H, Lee B-K. Enhanced Coulomb counting method with adaptive SOC reset time for estimating OCV. *Proceeding of the 2014 IEEE Energy Conversion Congress and Exposition (ECCE)*. Pittsburg, PA, USA; 2014:1313-1318.
32. Jaguemont J, Nikolian A, Omar N, Goutam S, Van Mierlo J, Van den Bossche P. Development of a two-dimensional-thermal model of three battery chemistries. *IEEE Trans Energy Convers.* 2017;32:1447-1455.
33. Tan YK, Mao JC, Tseng KJ. Modelling of battery temperature effect on electrical characteristics of Li-ion battery in hybrid electric vehicle. *Proceeding of the 2011 IEEE Ninth International Conference on Power Electronics and Drive Systems*. Singapore; 2011:637-642.
34. Xie Y, Wang X, Hu X, et al. An enhanced electro-thermal model for ev battery packs considering current distribution in parallel branches. *IEEE Trans Power Electron.* 2022;37(1):1027-1043.
35. Morganti MV, Longo S, Tirovic M, Blaise CY, Forostovsky G. Multi-scale, electro-thermal model of NMC battery cell. *IEEE Trans Veh Technol.* 2019;68:10594-10606.
36. Zhang L, Lyu C, Hinds G, et al. Parameter sensitivity analysis of cylindrical  $\{\text{LiFePO}_4\}_4$  battery performance using multi-physics modeling. *J Electrochem Soc.* 2014;161:A762-A776.
37. A123 lithium iron phosphate (LFP). [Online]. <http://www.a123systems.com/automotive/products/cells/>
38. Akbarabadi SA, Atighechi H, Jatskevich J. Circuit-averaged and state-space-averaged-value modeling of second-order flyback converter in CCM and DCM including conduction losses. *Proceeding of the 2013 IEEE 4th International Conference on Power Engineering, Energy and Electrical Drives*. Istanbul, Turkey; 2013:995-1000.
39. Cao Y, Li K, Lu M. Balancing method based on flyback converter for series-connected cells. *IEEE Access.* 2021;9:52393-52403.
40. Erickson R. *Fundamentals of Power Electronics*. Springer Science & Business Media; 2007.

41. Brandis A, Pelin D, Topić D, Tomašević B. Active li-ion battery charge balancing system based on flyback converter. *Proceeding of the 2020 IEEE 11th International Symposium on Power Electronics for Distributed Generation Systems (PEDG)*. Dubrovnik, Croatia; 2020:164-169.
42. Chai T, Draxler RR. Root mean square error (RMSE) or mean absolute error (MAE)?—arguments against avoiding RMSE in the literature. *Geosci Model Dev*. 2014;7: 1247-1250.

**How to cite this article:** Zabetian-Hosseini A, Ghazanfari A, Boulet B. A finite-state machine-based control design for thermal and state-of-charge balancing of lithium iron phosphate battery using flyback converters. *Battery Energy*. 2024;3:20230055. doi:10.1002/bte2.20230055